Full Text View

Volume 28, Issue 7 (July 1998)

Journal of Physical Oceanography
Article: pp. 1534–1551 | Abstract | PDF (431K)

Nonlinear Evolution of Surface Wave Spectra on a Beach

C. A. Norheim and T. H. C. Herbers

Department of Oceanography, Naval Postgraduate School, Monterey, California

Steve Elgar

Electrical Engineering and Computer Science, Washington State University, Pullman, Washington

(Manuscript received June 30, 1997, in final form October 28, 1997)

DOI: 10.1175/1520-0485(1998)028<1534:NEOSWS>2.0.CO;2

ABSTRACT

The shoaling evolution of wave spectra on a beach with straight and parallel depth contours is investigated with a stochastic Boussinesq model. Existing deterministic Boussinesq models cast in the form of coupled evolution equations for the amplitudes and phases of discrete Fourier modes describe accurately the shoaling process for arbitrary incident wave conditions, but are numerically cumbersome for predicting the evolution of continuous spectra of natural wind-generated waves. The stochastic formulation used here, based on the closure hypothesis that phase coupling between quartets of wave components is weak, predicts the shoaling evolution of the continuous frequency spectrum and bispectrum of the wave field. The general characteristics of the stochastic model and the dependence of wave shoaling on nonlinearity, initial spectral shape, and bottom profile are illustrated with numerical simulations. Predictions of stochastic and deterministic Boussinesq models are compared with data from a natural barred ocean beach. Both models accurately reproduce the observed nonlinear wave transformation for a range of conditions.

1. Introduction

Wind-generated surface gravity waves are the principal driving force of nearshore fluid motions (e.g., longshore currents, rip currents, and undertow) and sediment transport (e.g., erosion and accretion of beaches, and the formation of bars and cusps). As waves shoal onto beaches, amplitudes increase, wavelengths decrease, and directions refract toward normal incidence. These linear propagation effects are observed readily and understood well. Additionally, pronounced nonlinear effects in shallow water cause a

dramatic transformation of wave shapes from initially symmetric, nearly sinusoidal profiles, to asymmetric, pitched forward profiles characteristic of near-breaking waves. The mechanism for this transformation is nonlinear triad interactions in which two primary wave components with frequencies ω_1 and ω_2 excite a secondary wave component with the sum ($\omega_1 + \omega_2$) or difference ($\omega_1 - \omega_2$) frequency. The nonlinearly excited secondary wave components are phase-locked to the statistically independent primary wave components incident from deep water, and thus cause deviations from Gaussian statistics (e.g., steep and asymmetric wave profiles). Even relatively weak secondary components change significantly the shapes of waves in shallow water. Whereas the incident waves and the nonlinearly excited higher frequency waves are predominantly dissipated in the surf zone, the nonlinearly excited lower frequency (infragravity) wave components reflect from the beach and often dominate wave runup at the shoreline.

In deep ($\kappa h \gg 1$, where κ is the wavenumber magnitude and h is the water depth) and intermediate [$\kappa h = O(1)$] water depths triad interactions are nonresonant. The nonlinearly excited secondary waves remain small ("bound" waves) and are described well by finite depth theory based on the Stokes perturbation expansion for small wave steepness (Phillips 1960; Hasselmann 1962;Herbers et al. 1992, 1994; and many others). In shallow water ($\kappa h \ll 1$) triad interactions are near resonant, and finite depth theory is valid only for small values of the Ursell number, $\mathrm{Ur} \equiv a/(\kappa^2 h^3)$ (Ursell 1953) where a is the wave amplitude. Models for wave propagation in shallow water on natural beaches are usually based on the Boussinesq equations (Peregrine 1967) that assume both a/h (nonlinearity) and $(\kappa h)^2$ (dispersion) are small and of the same order [i.e., $\mathrm{Ur} = O(1)$]. Freilich and Guza (1984) developed a frequency domain (i.e., neglecting directional spreading effects) Boussinesq model that is initialized at an offshore boundary by a discrete Fourier representation of the incident waves. A coupled set of evolution equations for the amplitudes and phases of the Fourier modes is solved numerically to predict the shoaling transformation of the wave train. Spectral statistics are obtained by averaging, either over many sets of initial conditions or over adjacent frequency bands for one long initial time series. This model predicts accurately the energy transfers to higher frequencies and associated wave shape changes on natural beaches, even for large Ur values observed in near-breaking waves (Elgar and Guza 1985a; Elgar et al. 1990a, 1997). Numerous other frequency and time domain formulations of Boussinesq models have been developed that incorporate improved dispersion relations (e.g., Madsen et al. 1991), two-dimensional topographic effects (e.g., Liu et al. 1985), stronger nonlinearity (e.g., Wei et al. 1995), and parameterizations of wave breaking effects (e.g., Schäffer et al. 1993). Although the wave shoaling process is described accurately, these essentially deterministic models are cumbersome for predicting spectra of natural random waves, requiring large computing resources and a detailed specification of incident wave conditions at the offshore boundary that often is not available.

Recently, stochastic formulations of shallow water wave models were introduced that predict the evolution of wave spectra based on an energy balance equation, analogous to spectral models used in deep water (e.g., The WAMDI Group 1988). Abreu et al. (1992) developed a model for the evolution of the frequency–directional wave spectrum based on an asymptotic second-order closure for nondispersive waves (Newell and Aucoin 1971). In this model phase coupling between wave triads (i.e., non-Gaussian statistics) is neglected. Eldeberky and Battjes (1995) used Boussinesq equations and a simple parameterization of phase coupling in near-resonant wave triads to develop a similar second-order closure model (for unidirectional waves) that is more appropriate for the weakly dispersive regime and typically short interaction distances of sloping beaches. Herbers and Burton (1997) derived a third-order closure Boussinesq model for directionally spread waves propagating over a gently sloping beach with straight and parallel depth contours. This weakly non-Gaussian model is based on the hypothesis that phase-coupling between quartets of wave components is weak, and consists of a coupled set of evolution equations for the wave spectrum and bispectrum. The bispectrum describes the degree of coupling and the phase relationship in triads of nonlinearly interacting wave components (Hasselmann et al. 1963). In deep and intermediate water depths, the bispectrum is completely determined by the local spectrum, and enables the detection of relatively weak phase-coupled, forced secondary waves that are concealed in the spectrum by more energetic freely propagating primary waves (e.g., Hasselmann et al. 1963; Masuda and Kuo 1981; Herbers et al. 1992, 1994). In shallow water, the bispectrum evolves strongly and describes statistically the shapes of shoaling waves (e.g., Elgar and Guza 1985b; Elgar et al. 1990a).

Here, a one-dimensional (i.e., directional spreading effects are neglected) numerical implementation of the third-order closure model of Herbers and Burton (1997) is presented. This formulation allows for simple illustration of stochastic model characteristics and comparisons with field data and existing one-dimensional deterministic models. Energy transfers to higher frequencies via sum triad interactions are insensitive to directional spreading angles of incident waves (Herbers and Burton 1997, and references therein), and thus can be accurately predicted with a one-dimensional model. However, energy transfers to infragravity frequencies in difference triad interactions are reduced significantly for large directional spreading angles (Herbers et al. 1995a;Herbers and Burton 1997). Additionally, the reflection of infragravity waves from shore (Elgar et al. 1994) and from turning points on the sloping beach and shelf (Herbers et al. 1995b), and the associated amplification of edge wave modes (Huntley 1976; Bowen and Guza 1978) is neglected. Hence, infragravity waves are represented only crudely in the present model formulation.

The stochastic formulation of the Boussinesq wave shoaling equations is reviewed in section 2, followed by a description of the numerical model implementation. The dependence of wave shoaling evolution on nonlinearity, spectral shape of incident waves, and the beach profile is examined through numerical simulations in section 3. Stochastic and deterministic

(the Freilich and Guza 1984 model) Boussinesq predictions are compared with data collected on a natural beach near Duck, North Carolina, in section 4, followed by conclusions in section 5.

2. A stochastic Boussinesq model

Herbers and Burton (1997) derived a stochastic formulation of the Boussinesq wave shoaling equations for directionally spread waves propagating on a beach with straight and parallel depth contours. Under the third-order closure hypothesis that phase coupling between quartets of wave components is weak, the statistical properties of the waves are described by a coupled set of evolution equations for the frequency (ω)–alongshore wavenumber (l) spectrum $E(\omega, l)$ and bispectrum $B(\omega', l', \omega - \omega', l - l')$. If directional spreading is neglected (i.e., $l = 0$), these equations [(22a) and (22b) in Herbers and Burton 1997] reduce to

$$\frac{d}{dx}E(\omega) = -\frac{1}{2h}\frac{dh}{dx}E(\omega) + \frac{3\omega}{2h^{3/2}g^{1/2}} \times \int_{-\infty}^{\infty} \mathrm{Im}\{B(\omega', \omega - \omega')\}\, d\omega' \qquad (1a)$$

$$\frac{d}{dx}B(\omega', \omega - \omega') = \left(-\frac{3}{4h}\frac{dh}{dx} - i\frac{h^{1/2}\omega'(\omega - \omega')\omega}{2g^{3/2}}\right) \times B(\omega', \omega - \omega') - i\frac{3}{2h^{3/2}g^{1/2}} \times [\omega' E(\omega - \omega')E(\omega) + (\omega - \omega')E(\omega')E(\omega) - \omega E(\omega')E(\omega - \omega')], \qquad (1b)$$

where the x axis points onshore $E(\omega)$ and $B(\omega', \omega - \omega')$ are the frequency spectrum and bispectrum respectively, $h(x)$ is the water depth, g is gravity, and Im{ } indicates the imaginary part. The integrals of E and B over all frequencies yield respectively, the mean square $\langle\eta^2\rangle$ and mean cube $\langle\eta^3\rangle$ of the surface elevation function $\eta(x, t)$.

The first term on the right-hand side of (1a) and (1b) represents linear shoaling effects. The nonlinear transfers in the energy spectrum are controlled by the imaginary part of the bispectrum [the integral on the right-hand side of (1a)]. The energy product terms in (1b) represent the changes in the imaginary part of the bispectrum owing to the three possible nonlinear interactions (one sum interaction and two difference interactions) within the $(\omega', \omega - \omega', \omega)$ triad. The second term on the right-hand side of (1b) represents the detuning of the interactions from resonance (i.e., changes in the phase of the bispectrum) caused by weak dispersion. In the limit of small amplitudes and bottom slope, solutions for $E(\omega)$ and $B(\omega', \omega - \omega')$ smoothly match the second-order bound-wave solutions of dispersive finite depth theory (Herbers and Burton 1997).

Initialization of the model requires only a spectrum $E(\omega)$ at the offshore boundary of the model domain (e.g., from nearby measurements or a regional model prediction). The corresponding initial bispectrum $B(\omega', \omega - \omega')$ is approximated by the second-order finite depth theory expression (Hasselmann 1962; Hasselmann et al. 1963):

$$B(\omega', \omega - \omega') = 2[D(\omega', \omega - \omega')E(\omega')E(\omega - \omega') + D(\omega', -\omega) \times E(\omega')E(\omega) + D(\omega - \omega', -\omega)E(\omega - \omega')E(\omega)] \qquad (2)$$

with the coupling coefficient D given by

$$g(\kappa_1 + \kappa_2) \tanh[(\kappa_1 + \kappa_2)h] - (\omega_1 + \omega_2)^2$$

$$\times \left\{ \frac{\omega_1\omega_2}{g} - \frac{g\kappa_1\kappa_2}{\omega_1\omega_2} - \frac{g}{2(\omega_1 + \omega_2)} \times \left(\frac{\kappa_1^2}{\omega_1 \cosh^2(\kappa_1 h)} + \frac{\kappa_2^2}{\omega_2 \cosh^2(\kappa_2 h)} \right) \right\}$$

$$+ \frac{\omega_1^2 + \omega_1\omega_2 + \omega_2^2}{2g} - \frac{g\kappa_1\kappa_2}{2\omega_1\omega_2}, \qquad (3)$$

where h is the local water depth and the frequencies ω_1, ω_2 and wavenumbers κ_1, κ_2 ($\kappa_i < 0$ for $\omega_i < 0$) of the interacting primary wave components obey the linear theory dispersion relation $\omega^2_i = g\kappa_i \tanh(\kappa_i h)$. In this approximation third-order statistics associated with the coupling between free wind-generated waves and bound secondary waves are completely specified by the local wave spectrum and water depth. Bispectra of waves observed in intermediate water depths [$\kappa h = O(1)$] agree with Eqs. (2), (3) (Hasselmann et al. 1963;Herbers et al. 1992, 1994). Alternatively, the stochastic evolution equations (1a,b) may be initialized with measurements of both $E(\omega)$ and $B(\omega', \omega - \omega')$, but in many applications such detailed offshore boundary conditions are not available because operational global and regional wave models (e.g., The WAMDI Group 1988) assume Gaussian wave statistics (i.e., $B = 0$) and routine wave measurements from buoy networks lack the accuracy to quantify weak second-order wave properties.

Using the symmetry relations (Hasselmann et al. 1963)

$$\begin{aligned} E(\omega) &= E(-\omega) \\ B(\omega', \omega - \omega') &= B(\omega - \omega', \omega') = B^*(-\omega', \omega' - \omega) \\ &= B(\omega', -\omega) = B(\omega - \omega', -\omega), \end{aligned}$$

where the asterisk indicates the complex conjugate, the integral term in (1a) can be expressed as the sum of two integrals over positive frequencies

$$\int_{-\infty}^{\infty} \mathrm{Im}\{B(\omega', \omega - \omega')\}\, d\omega' = \int_0^{\omega} \mathrm{Im}\{B(\omega', \omega - \omega')\}\, d\omega' - 2\int_0^{\infty} \mathrm{Im}\{B(\omega', \omega)\}\, d\omega' \qquad (4)$$

that represent the energy transfers to frequency ω resulting from sum interactions of $(\omega', \omega - \omega')$ wave pairs and difference interactions of $(\omega + \omega', \omega')$ wave pairs, respectively. Hence, integrations of the spectrum and bispectrum evolution equations (1a,b) can be restricted to positive frequencies (ω', $\omega - \omega'$, $\omega > 0$).

The spectrum and bispectrum are discretized:

$$\begin{aligned} \omega_n &= n\Delta\omega \quad \text{for } n = 1, 2, \cdots, N \\ E_n &= E(\omega_n) \quad \text{for } n = 1, 2, \cdots, N \\ B_{nm} &= R_{nm} + iI_{nm} = B(\omega_n, \omega_m) \\ &\quad \text{for } n = 1, 2, \cdots, N-1 \quad \text{and} \\ &\quad m = 1, 2, \cdots, N - n, \end{aligned}$$

where $\Delta\omega$ is the bandwidth and ω_N the highest frequency included in the computations. With these definitions, (1a,b) reduce to a linear set of N^2 ordinary differential equations that can be written in the general form

$$\frac{d\mathbf{Y}}{dx} = \mathbf{F}(\mathbf{Y}),$$

where the elements of **Y** are the discretized spectrum (E_n) and bispectrum (R_{nm}, I_{nm}), and **F**(**Y**) incorporatesthe corresponding right-hand side of (1a), (1b). This system of equations is solved using the Bulirsch and Stoer (1966) method, a variant of Richardson extrapolation to the limit that uses adaptive stepsize control (Press et al. 1992).

3. Simulations

To examine the general model characteristics and the dependence of wave shoaling evolution on nonlinearity, initial spectral shape, and bottom profile, numerical simulations were carried out with incident wave spectra given by

$$E_1(f) = E\frac{\alpha}{f_p}\exp\left[\frac{\alpha}{1-\alpha}\left(\frac{f}{f_p}\right)^{1-\alpha}\right]\left(\frac{f}{f_p}\right)^{-\alpha} \qquad (5a)$$

$$E_2(f) = E\frac{\alpha}{\pi f_p}\operatorname{sech}\left[\alpha\frac{f-f_p}{f_p}\right], \qquad (5b)$$

where $E_1(f)$ and $E_2(f)$ are single-sided spectra [$E(f) = 4\pi E(\omega)$ with $f = \omega/2\pi$], E is the surface elevation variance $\langle\eta^2\rangle$, and the parameter α defines the width of the spectrum. All model simulations were initialized in a depth h = 6 m with a spectral peak frequency f_p = 0.07 Hz. The corresponding wavenumber k_p = 0.058 m^{-1}, and thus $k_p h$ = 0.35 at the offshore boundary. Example simulations of the shoaling of a broad sea spectrum [E_1 with α = 5, the Pierson–Moskowitz (1964) spectral shape] and a narrow swell spectrum (E_2 with α = 20, the full width at half maximum power is 0.009 Hz) are shown in Figs. 1–5 for different bottom profiles and significant wave heights ($H_s \equiv 4E^{1/2}$). The initial bispectrum was obtained by substituting the initial spectrum in the finite depth theory relation (2). The number of frequencies N in the computations is 250 with a bandwidth Δf = 0.0016 Hz and a maximum frequency f_N = 0.4 Hz. The model results (both spectral and bispectral predictions) are insensitive to the choice of Δf as long as the initial spectrum is well resolved. Although the highest frequency components are strongly dispersive at the offshore boundary, the model predictions are insensitive to the choice of f_N because the large mismatch from resonance of triad interactions involving high-frequency components inhibits nonlinear energy transfers (see Freilich and Guza 1984; Herbers and Burton 1997 for further discussion).

The shoaling evolution of narrow swell spectra with significant wave heights of 0.05 and 0.5 m on plane beaches with slopes of 1:30 and 1:300 is shown in Fig. 1. All four simulations show the growth of peaks at harmonic frequencies ($2f_p$, $3f_p$, . . .) and an infragravity peak at about 0.01 Hz. Even for the small H_s = 0.05 m waves, harmonic spectral levels are significant (up to 10% of the primary peak level) in 1.5-m depth. Although the nonlinearity remains weak ($[2E]^{1/2}/h$, a representative value of a/h, ranges between 0.003 and 0.017), the Ursell number (Ur = $[2E]^{1/2}/[k_p^2 h^3]$) increases from 0.024 in 6-m depth to a relatively large value of 0.58 in 1.5-m depth. As expected, the shoaling evolution is much stronger for the larger H_s = 0.5 m waves, with harmonic spectral levels that are comparable with the primary peak levels in 1.5-m depth. In these simulations a/h increases from 0.03 in 6-m depth to 0.17 in 1.5-m depth, and Ur increases from 0.24 to 5.8. In both the H_s = 0.05 and 0.5 m cases, stronger growth of harmonic and infragravity peaks is predicted on a gentle (1:300) slope than on a steep (1:30) slope. Eventually (Figs. 1d, 1f) nonlinear energy transfers fill the valleys between harmonic peaks and the spectrum flattens, similar to simulations with a deterministic Boussinesq model (Elgar et al. 1990b).

The dependence of nonlinear interactions on the bottom slope is further illustrated in Fig. 2 with normalized bispectrum predictions in 2-m depth. The normalized bispectrum

$$b(f_1, f_2) \equiv \frac{B(f_1, f_2)}{[E(f_1)E(f_2)E(f_1 + f_2)]^{1/2}}, \qquad (6)$$

with $B(f_1, f_2) \equiv 8\pi^2 B(\omega_1, \omega_2)$, is a relative measure of phase coupling between wave components with frequencies f_1, f_2, and $f_1 + f_2$ (Herbers et al. 1992). The predominantly positive values of the imaginary part of the bispectrum at sum frequencies $f_1 + f_2 > 0.1$ Hz indicate energy transfers to higher frequencies through sum interactions, whereas negative values at lower sum frequencies indicate energy transfers to lower (infragravity) frequencies through difference interactions [(1a), (4)]. All four simulations show strong coupling at $(f_1, f_2) = (0.07, 0.07)$ Hz (the f_p, f_p, $2f_p$ interaction) and at (0.07, 0.14) Hz (the f_p, $2f_p$, $3f_p$ interaction). The larger wave and gentle bottom slope simulations also show coupling to higher harmonics [e.g., the (0.14, 0.14), (0.21, 0.07), and (0.21, 0.14) Hz peaks]. Whereas the imaginary part of b is small compared with the real part of b on the gentle (1:300) slope (i.e., peaked, but nearly symmetric wave shapes, Elgar and Guza 1985b), the real part of b is relatively small on the steep (1:30) slope (i.e., pitched forward wave shapes).

Simulation results of the shoaling of a broad spectrum with the same initial significant wave heights (0.05 and 0.5 m) and beach slopes (1:30 and 1:300) are shown in Fig. 3. The spectral evolution is much weaker than in the narrow spectra simulations because a principal effect of triad interactions is to spread energy to frequencies where spectral levels are relatively low. In the $H_s = 0.05$ m simulations (Figs. 3a, 3c, 3e) the nearly uniform increase in spectral levels at frequencies above about 0.05 Hz is a linear shoaling (conservation of lowest-order energy flux) effect [the first term on the right-hand side of (1a)]. The 1:300 slope simulation shows slightly larger growth of spectral levels above about $2f_p$ that is the result of sum interactions. The larger wave ($H_s = 0.5$ m) simulations (Figs. 3b, 3d, 3f) show the expected stronger nonlinear evolution. Although harmonic peaks do not develop in a broad spectrum, nonlinear interactions cause a flattening to a nearly white spectrum in 1.5-m depth, similar to the narrow spectrum simulations (Fig. 1f). The dependence on bottom slope is similar to that for the narrow spectrum (Fig. 1), with larger cumulative energy transfers on a gently sloping beach (compare the solid with dashed curves in Fig. 3).

The shoaling evolution of a broad spectrum of waves (initial $H_s = 0.5$ m) over three different bottom profiles is compared in Fig. 4. All three profiles start with a gentle (1:300) slope from a depth of 6 to 3 m to let the waves evolve to a shallow water regime with significant nonlinear energy transfers. From 3-m depth shoreward, the waves either continue to shoal on a 1:300 slope to 1-m depth (“plane beach” case), propagate the same 600-m distance in (constant) 3-m depth (“flat section” case), or unshoal over a −1:200 section back to 6-m depth (“barred” case). Energy transfers to higher frequencies between $x = 900$ and 1500 m are notably smaller on the flat section than on the plane beach, and on the downslope section of the barred profile high-frequency spectral levels are reduced by almost an order of magnitude to approximately the initial levels in 6-m depth. This decrease is about a factor of 3 larger than the linear unshoaling effect associated with the increase in group speed between depths of 3 and 6 m [the first term on the right-hand side of Eq. (1a)] and results primarily from nonlinear energy transfers [the second term on the right-hand side of Eq. (1a)] to other parts of the spectrum. At infragravity frequencies spectral levels continue to increase on all three profiles, but the growth is strongest on the plane beach and weakest on the barred profile (Fig. 4).

Bispectra after 150 m of evolution on the three different bottom profiles are compared in Fig. 5. The small positive imaginary part of the bispectrum predicted at $x = 900$ m for sum frequencies $f_1 + f_2 > 0.15$ Hz (Fig. 5a) remains positive on the plane beach (Fig. 5b), indicating continued energy transfers to high frequencies [(1a), (4)]. On the flat section where the spectral evolution is weak, the imaginary part of the bispectrum shows small alternating positive and negative peaks (Fig. 5c). On the downslope section of the barred profile, positive values of the imaginary part of the bispectrum evolve to negative values over a wide range of frequencies (Fig. 5d), indicating that a reversal in nonlinear energy transfers toward lower frequencies [(1a), (4)] causes the predicted decrease in high-frequency spectral levels on the downslope. At sum frequencies $f_1 + f_2 < 0.1$ Hz the imaginary part of b remains negative in all cases [the blue peak at (0.01, 0.06) Hz] indicating energy transfers from the spectral peak to infragravity frequencies.

In simulations of waves propagating either over a flat bottom or over a bar into deeper water (Fig. 4), small undulations appear in the spectra that grow with distance. A sensitivity analysis of the numerical solutions to variations in frequency bandwidth, the error tolerance of the numerical integration routine, the maximum frequency, and different extrapolation techniques (i.e., polynomial and rational extrapolation) yielded identical features in all calculations. Energy was also conserved in the simulations to a high degree of accuracy. These numerical tests indicate that the predicted growing undulations in the spectrum are true features of the spectral and bispectral evolution equations and not caused by numerical truncation errors. However, the Boussinesq equations are truncated at second-order in nonlinearity and thus are valid only over $O(a/h)^{-1}$ distances (Freilich and Guza 1984). The statistical closure approximation (Herbers and Burton 1997) may contribute additional errors to the predicted evolution of these moderately energetic waves over long distances. Hence, the undulations in the spectrum may not be physically real, but result possibly from the breakdown of the approximations used in the present model.

4. Comparisons with field observations

Field observations of wave shoaling were obtained with a cross-shore transect of 15 colocated pressure transducers, bidirectional electromagnetic current meters, and sonar altimeters deployed on a sandy, barred beach near Duck, North Carolina (Elgar et al. 1997). The transect extended 350 m from the shoreline to about 6-m depth (Fig. 6). The sample frequency of all instruments was 2 Hz. Sea-surface elevation spectra with approximately 120 degrees of freedom were estimated from three-hour-long pressure records using a linear theory depth correction.

The present analysis of four case studies is focused on benign wave conditions (0.4 m < H_s < 0.8 m in 6-m depth) when the surf zone was confined to the beach face at the shoreward end of the transect. These observations span a 2-week period in September 1994 with small bathymetric changes. Differences between the depth profiles of the case studies (Fig. 6) result primarily from tidal sea level fluctuations. The beach profile includes a sandbar located about 120–140 m from the shoreline and submerged approximately 2.2–2.5 m below the mean sea surface. The bottom slope is approximately 1:80 seaward of the sandbar. Shoreward of the sandbar, the seafloor elevation decreases slightly (20–40 cm) into a relatively flat trough 80 m wide that extends to the steep (1:10) beach face. The beach profiles used in the Boussinesq model computations were obtained through linear interpolation of the depth estimates from the sonar altimeter measurements (Gallagher et al. 1998).

Stochastic Boussinesq model predictions of wave spectrum evolution for the four case studies are compared with the observed spectrum evolution and that predicted by the deterministic Boussinesq model of Freilich and Guza (1984) in Figs. 7, 8, 12, and 15. Initial spectra of the stochastic model predictions for 15, 21, and 24 September were calculated from observations made at the farthest offshore pressure sensor (x = 0). The 10 September case was initialized with observations from x = 80 m. As in the simulations, the initial bispectrum was obtained from second-order finite depth theory by substituting the initial spectrum into Eq. (2). In all cases these predicted initial bispectra (not shown) are in good agreement with bispectra estimated from the measured pressure time series at the farthest offshore sensors. A model discretization with a frequency bandwidth Δf = 0.006 Hz and a maximum frequency f_N = 0.42 Hz was used to resolve adequately the initial observed spectra and capture the subsequent nonlinear spectral evolution over a wide frequency range.

The deterministic model was initialized (at the same offshore sensor locations as the stochastic model) with measured pressure time series, and thus incorporates higher-order statistics of incident waves without any approximations. The three-hour-long incident wave records were subdivided into ten 1024-s segments. The Fourier amplitudes (corrected to surface displacements with a linear theory depth correction) and phases of each segment were transformed to shoreward locations with the coupled evolution equations (23a,b) in Freilich and Guza (1984). A slightly lower cutoff frequency (0.35 Hz) was used because the stronger dispersion approximation of these equations yields imaginary wavenumbers in deep water. The resulting spectra were ensemble averaged and smoothed over six neighboring bands to obtain spectra with the same resolution as the stochastic model predictions. The predictions of both the stochastic and deterministic models are insensitive to the details of the discretization of incident wave conditions.

In all four cases (and other case studies not shown) predictions of both models agree well with the observed wave shoaling evolution. The narrow swell cases (10 and 15 September) show the amplification of harmonic peaks. On 10 September the incident wave spectrum was dominated by swell with a peak frequency $f_p \approx$ 0.075 Hz, with a broader, but relatively small sea peak at 0.12 Hz (Fig. 7). Energy is transferred from the swell peak frequency f_p to higher frequencies through sum triad interactions, resulting in distinct harmonic peaks at $2f_p$ (0.15 Hz; driven by f_p, f_p interactions), $3f_p$ (0.23 Hz; f_p, $2f_p$ interactions), and $4f_p$ (0.3 Hz; f_p, $3f_p$ and $2f_p$, $2f_p$ interactions). Close to shore the small 0.12-Hz incident sea peak is completely submerged in the $2f_p$ swell harmonic (Fig. 7f).

On 15 September the incident wave spectrum was bimodal with nearly equal energy in a narrow swell peak ($f_p \approx$ 0.06 Hz) and a slightly broader peak at twice the swell frequency ($2f_p \approx$ 0.12 Hz) (Fig. 8). The observed bispectrum at x = 0 (not shown) does not indicate significant phase coupling between (f_p, f_p, $2f_p$) triads, suggesting that the waves at 0.06 and 0.12 Hz were freely propagating swells arriving from two different storms. As these waves propagate over the shallow sandbar, nonlinear energy transfers in sum interactions yield clearly distinguishable peaks at $3f_p$, $4f_p$, and $5f_p$ (compare Fig. 8a with 8c). The cross-shore evolution of spectral levels at frequencies f_p, $2f_p$, $3f_p$, $4f_p$, and $5f_p$ is shown in Fig. 9. High-frequency spectral levels observed and predicted by both models are approximately constant between x = 0 and 150 m because a large mismatch from resonance inhibits nonlinear energy transfers. Large nonlinear energy transfers to high frequencies are observed and predicted on the sandbar (x = 200–300 m) where the decrease in water depth has reduced the mismatch of triad interactions from resonance. Partial reflection of the 0.06 Hz swell from the beach is evident in the large cross-shore energy variations (i.e., standing wave patterns) observed close to shore. Good agreement between the observed and predicted growth of higher-frequency harmonics indicates that nonlinear energy transfers are insensitive to weak reflections from shore (Elgar et al. 1997).

Both the observed and predicted bispectra on 15 September show the expected shoaling transition from real values (i.e., wave profiles with symmetric, peaked crests and flat troughs) (Figs. 10a and 10b) to imaginary values (i.e., wave profiles with asymmetric, pitched-forward crests) (Figs. 10c and 10d). Although the observed and predicted bispectra are similar, they differ in detail at the shallower sites (Fig. 11). In frequency pairs involving the 0.06-Hz swell peak, the observed bispectrum shows a dramatic shift from imaginary to real values between x = 320 and 335 m that is absent in the model predictions. This biphase shift is likely caused by the partial reflection of the 0.06 Hz swell from shore (Fig. 9) that is not incorporated in the model predictions. Midway between nodes and antinodes (e.g., x = 320 m) the incident and reflected components are 90° out of phase, causing large biphase shifts in triads involving the standing wave component.

The waves observed on 24 September were more energetic than the two cases of swell discussed above and had a broader spectrum with a peak frequency $f_p \approx 0.1$ Hz (Fig. 12). Sum interactions transfer energy to a wide range of higher frequencies, causing a broadening of the spectrum rather than the development of distinct harmonic peaks observed on 10 and 15 September. The observed and predicted spectral levels at $3f_p$ decrease sharply between the bar crest (x = 240 m) and the slightly deeper trough (x = 300 m), whereas energy levels at $2f_p$ continue to increase (Fig. 13). These results suggest that energy is transferred back to lower frequencies as waves travel over the sandbar into deeper water and are consistent with the simulations of waves propagating over a barred beach (Figs. 4 and 5). Observed and predicted bispectra show a clear transition from positive imaginary parts seaward of the bar crest (Figs. 14a and 14b) to negative imaginary parts shoreward of the bar crest (Figs. 14c and 14d) that is consistent with a reversal in the nonlinear energy transfer [(1a), (4)].

In contrast to the 10, 15, and 24 September case studies, the shoaling evolution of the broad, featureless spectrum observed on 21 September (Fig. 15) is weak. The nonlinearity is comparatively strong (H_s = 0.8 m), but sum and difference interactions tend to cancel in this almost white spectrum (1b). Predicted bispectral levels (not shown) are low, consistent with the observations.

Discrepancies between observations and predictions are roughly comparable for the two models (spectral levels agree within about a factor of 4), but differ in detail. Close to the initial conditions the deterministic model tends to overpredict energy transfers to higher frequencies, whereas the stochastic model predictions agree with the observed spectra (e.g., Figs. 7a–c and 8a–b). Farther from the initial conditions the stochastic model tends to overpredict high-frequency spectral levels, whereas the deterministic model predictions are close to (e.g., Figs. 7e–f and 8e–f), or in some cases, lower than (e.g., Figs. 12c–d) the observed spectral levels. Some of these differences may be the result of the different dispersion relationships (discussed in detail in Freilich and Guza 1984) used in the two models. Except at very high frequency where it diverges from linear finite depth theory, the stronger dispersion approximation used in the deterministic model yields a more accurate linear energy balance than the weaker dispersion approximation used in the stochastic model. However, the approximation of dispersion characteristics also affects the nonlinear terms in the equations with implications for the predicted harmonic growth that are not fully understood. Based on comparisons with field data, Freilich and Guza (1984) show that harmonic growth is overpredicted by models that use the weak dispersion approximation and underpredicted by models that use the stronger dispersion approximation, qualitatively consistent with the present results.

Other possible explanations for small differences between the deterministic and stochastic model predictions include the statistical closure of the stochastic model and the different way the models are initialized. The spectra predicted by the stochastic model, based on statistically averaged equations and an initially smooth bispectrum, are smoother than the spectra predicted by the deterministic model, which show some possibly spurious structure at higher frequencies that likely is caused by the statistical uncertainty of initial wave amplitudes and phases. Additionally, higher-order nonlinear effects and dissipation neglected in both models likely contribute significant errors in the predictions close to shore.

The predicted shoaling amplification of low-frequency (<0.06 Hz) spectral levels is in reasonable agreement with the observations, even though the model is obviously inadequate at infragravity frequencies as discussed in the introduction. Nevertheless, the roughly comparable observed and predicted infragravity energy levels suggest that nonlinear triad interactions are a plausible mechanism for the transfers of energy to infragravity frequencies in shallow water (Elgar and Guza 1985b; Herbers et al. 1995a).

5. Summary and conclusions

A stochastic model based on a third-order closure of the Boussinesq equations (Herbers and Burton 1997) for the shoaling of waves on a beach with straight and parallel depth contours is presented. The model includes nonlinear triad interactions in which two primary wave components with frequencies ω_1 and ω_2 excite a secondary wave component with the sum ($\omega_1 + \omega_2$) or difference ($\omega_1 - \omega_2$) frequency. Neglecting directional spreading effects, a coupled set of evolution equations for the wave spectrum and bispectrum is solved with standard numerical integration techniques. The model is numerically efficient and requires only an estimate of the incident wave spectrum for initialization. The bispectrum is initialized with a local

prediction based on second-order finite depth theory.

Numerical simulations were performed to examine the model characteristics and the dependence of predicted wave shoaling on nonlinearity, initial spectral shape, and bottom profile. In simulations with strong nonlinearity, both narrow and broad spectra tend to evolve to a flat featureless spectrum (Figs. 1f and 3f). Simulations of narrow spectra show the growth of harmonic peaks as the waves shoal. In simulations with broad spectra, comparable energy transfers to higher frequencies occur, but because the interactions are spread over a wide frequency range, the spectra remain featureless at high frequencies (Fig. 3). On steep bottom slopes, predicted bispectra have relatively large imaginary parts characteristic of pitched forward wave shapes, whereas the predominantly real bispectral values predicted on gentle slopes indicate symmetric, peaked wave shapes (Fig. 2). These characteristics are qualitatively consistent with wave shape evolution observed prior to breaking on natural beaches. The predicted cumulative spectral evolution is notably stronger on gently sloping beaches than on steep beaches (Figs. 1 and 3). Simulations of waves propagating over a bar into deeper water show a reversal in nonlinear energy transfers on the downslope section of the bar, with difference triad interactions transferring high-frequency energy back toward lower frequencies (Figs. 4 and 5).

Stochastic and deterministic (Freilich and Guza 1984) Boussinesq model predictions were compared with field observations of wave shoaling on a natural barred beach. Although predictions of the two models differ in detail, the overall agreement with the observed wave spectrum evolution is comparable. Both models predict accurately the nonlinear transfer of energy to higher frequencies for a range of incident wave conditions (Figures 7, 8, 12, and 15). These results are similar to earlier studies using deterministic Boussinesq models on plane and barred beaches (Freilich and Guza 1984; Elgar and Guza 1985a;Elgar et al. 1990a, 1997). Although spectral levels at high frequencies generally increase as waves propagate shoreward owing to sum triad interactions, in one case a decrease in high-frequency spectral levels was observed shoreward of the sandbar, consistent with difference interactions predicted by both models (Figs. 12–14). These observations support the simulation result that nonlinear interactions in a nonbreaking wave field can transfer high-frequency wave energy back to incident wave frequencies in regions of gradually increasing depth.

Acknowledgments

This research was supported by the Office of Naval Research (Coastal Dynamics Program). We thank R. T. Guza, E. L. Gallagher, B. Raubenheimer, and the staff of the Scripps Institution of Oceanography Center for Coastal Studies and the U.S. Army Corps of Engineers Field Research Facility for their contributions to the DUCK94 field data collection.

REFERENCES

Abreu, M., A. Larraza, and E. Thornton, 1992: Nonlinear transformation of directional wave spectra in shallow water. *J. Geophys. Res.*, **97,** 15 579–15 589..

Bowen, A. J., and R. T. Guza, 1978: Edge waves and surf beat. *J. Geophys. Res.*, **83,** 1913–1920..

Bulirsch, R., and J. Stoer, 1966: Numerical treatment of ordinary differential equations by extrapolation methods. *Numer. Math.*, **8,** 1–13..

Eldeberky, Y., and J. A. Battjes, 1995: Parameterisation of triad interactions in wave energy models. *Proc. Coastal Dynamics '95*, Gdansk, Poland, W. R. Dally and R. B. Zeidler, Eds., Amer. Soc. Civ. Eng., 140–148..

Elgar, S., and R. T. Guza, 1985a: Shoaling gravity waves: Comparisons between field observations, linear theory, and a nonlinear model. *J. Fluid Mech.*, **158,** 47–70..

— ,and — ,1985b: Observations of bispectra of shoaling surface gravity waves. *J. Fluid Mech.*, **161,** 425–448..

— ,M. H. Freilich, and R. T. Guza, 1990a: Model–data comparisons of moments of nonbreaking shoaling surface gravity waves. *J. Geophys. Res.*, **95,** 16 055–16 063..

— ,— ,and — ,1990b: Recurrence in truncated Boussinesq models for nonlinear waves in shallow water. *J. Geophys. Res.*, **95,** 11 547–11 556..

— ,T. H. C. Herbers, and R. T. Guza, 1994: Reflection of ocean surface gravity waves from a natural beach. *J. Phys. Oceanogr.*, **24,** 1503–1511..

— ,R. T. Guza, B. Raubenheimer, T. H. C. Herbers, and E. L. Gallagher, 1997: Spectral evolution of shoaling and breaking waves on a barred beach. *J. Geophys. Res.*, **102,** 15 797–15 805..

Freilich, M. H., and R. T. Guza, 1984: Nonlinear effects on shoaling surface gravity waves. *Philos. Trans. Roy. Soc. London,* **A311,** 1–41..

Gallagher, E. L., S. Elgar, and R. T. Guza, 1998: Observations of sand bar evolution on a natural beach. *J. Geophys. Res.,* **103,** 3203–3215..

Hasselmann, K., 1962: On the non-linear energy transfer in a gravity-wave spectrum, Part 1: General theory. *J. Fluid Mech.,* **12,** 481–500..

— ,W. Munk, and G. MacDonald, 1963: Bispectra of ocean waves. *Times Series Analysis,* M. Rosenblatt, Ed., John Wiley and Sons, 125–139..

Herbers, T. H. C., and M. C. Burton, 1997: Nonlinear shoaling of directionally spread waves on a beach. *J. Geophys. Res.,* **102,** 21 101–21 114..

— ,R. L. Lowe, and R. T. Guza, 1992: Field observations of orbital velocities and pressure in weakly nonlinear surface gravity waves. *J. Fluid Mech.,* **245,** 413–435..

— ,S. Elgar, and R. T. Guza, 1994: Infragravity-frequency (0.005–0.05 Hz) motions on the shelf. Part I: Forced waves. *J. Phys. Oceanogr.*, **24,** 917–927..

— ,— ,and — ,1995a: Generation and propagation of infragravity waves. *J. Geophys. Res.,* **100,** 24 863–24 872..

— ,— ,— ,and W. C. O'Reilly, 1995b: Infragravity-frequency (0.005–0.05 Hz) motions on the shelf. Part II: Free waves. *J. Phys. Oceanogr.,* **25,** 1063–1079..

Huntley, D. A., 1976: Long-period waves on a natural beach. *J. Geophys. Res.,* **81,** 6441–6449..

Liu, P. L.-F., S. B. Yoon, and J. T. Kirby, 1985: Nonlinear refraction–diffraction of waves in shallow water. *J. Fluid Mech.* **153,** 185–201..

Madsen, P. A., R. Murray, and O. R. Sørensen, 1991: A new form of the Boussinesq equations with improved linear dispersion characteristics. *Coastal Eng.,* **15,** 371–388..

Masuda, A., and Y.-Y. Kuo, 1981: Bispectra for the surface displacement of random gravity waves in deep water. *Deep-Sea Res.,* **28A,** 223–237..

Newell, A. C., and P. J. Aucoin, 1971: Semidispersive wave systems. *J. Fluid Mech.,* **49,** 593–609..

Peregrine, D. H., 1967: Long waves on a beach. *J. Fluid Mech.,* **27,** 815–827..

Phillips, O. M., 1960: On the dynamics of unsteady gravity waves of finite amplitude. Part 1: The elementary interactions. *J. Fluid Mech.,* **9,** 193–217..

Pierson, W. J., and L. Moskowitz, 1964: A proposed spectral form for fully developed wind seas based on the similarity theory of S. A. Kitaigorodskii. *J. Geophys. Res.,* **69,** 5181–5190..

Press, W. H., S. A. Teukolsky, W. T. Vetterling, and B. F. Flannery, 1992: *Numerical Recipes in FORTRAN: The Art of Scientific Computing.* 2d ed. Cambridge University Press, 963 pp..

Schäffer H. A., P. A. Madsen, and R. Deigaard, 1993: A Boussinesq model for waves breaking in shallow water. *Coastal Eng.,* **20,** 185–202..

Ursell, F., 1953: The long-wave paradox in the theory of gravity waves. *Proc. Cambridge Philos. Soc.,* **49,** 685–694..

The WAMDI Group, 1988: The WAM model: A third-generation ocean wave prediction model. *J. Phys. Oceanogr.,* **18,** 1775–1810..

Wei, G., J. T. Kirby, S. T. Grilli, and R. Subramanya, 1995: A fully nonlinear Boussinesq model for surface waves. Part I: Highly nonlinear, unsteady waves. *J. Fluid Mech.,* **294,** 71–92..

Figures

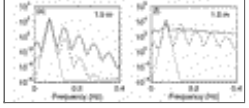

Click on thumbnail for full-sized image.

Fig. 1. Frequency spectra from numerical simulations of the shoaling evolution of a narrow spectrum of waves [(5b) with α = 20] over a plane beach. The stochastic model was initialized in 6-m depth. Predicted spectra are shown in depths 4 (upper panels), 2 (middle panels), and 1.5 m (lower panels) for incident wave significant heights of 0.05 (left panels) and 0.5 m (right panels) and beach slopes of 1:300 (solid curves) and 1:30 (dashed curves). The initial spectrum is indicated in each panel with a dotted curve.

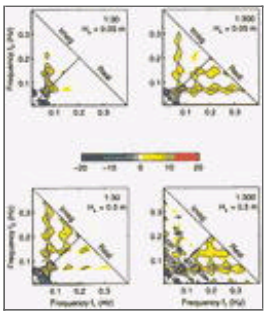

Click on thumbnail for full-sized image.

Fig. 2. Normalized bispectra $b(f_1, f_2)$ [(6), units $Hz^{-1/2}$] predicted in 2-m depth in the simulations described in Fig. 1. The real and imaginary parts of b are shown in the lower and left quadrants, respectively. Contour levels are: ±1, 3, and 5.

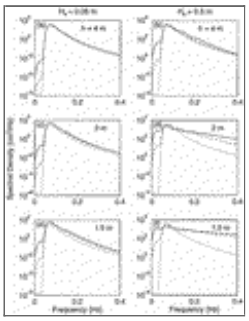

Click on thumbnail for full-sized image.

Fig. 3. Frequency spectra from numerical simulations of the shoaling evolution of a broad spectrum of waves [(5a) with α = 5] over a plane beach (same format as Fig. 1).

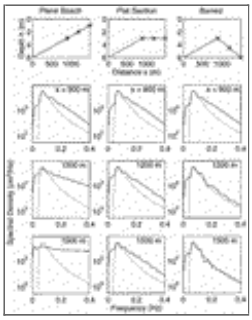

Click on thumbnail for full-sized image.

Fig. 4. Frequency spectra from numerical simulations of the evolution of a broad spectrum [(5a) with α = 5] over beaches with constant slope (left panels), a flat section (center panels), and a shallow submerged bar (right panels). Predictions are shown at x = 900, 1050, and 1200 m (indicated by asterisks on the bottom profiles in the upper panels). The dotted curve indicates the initial spectrum at x = 0 (h = 6 m, H_s = 0.5 m).

Click on thumbnail for full-sized image.

Fig. 5. Normalized bispectra predicted in the simulations described in Fig. 4: (a) x = 900 m (same for all 3 profiles), (b) x = 1050 m on the plane beach profile, (c) x = 1050 m on the flat section, and (d) x = 1050 m on the barred profile. The format of the panels is the same as in Fig. 2.

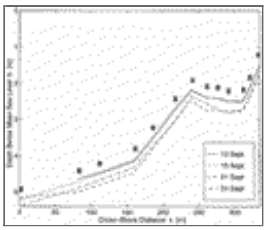

Click on thumbnail for full-sized image.

Fig. 6. Depth profiles and sensor locations (squares) of the four field data case studies.

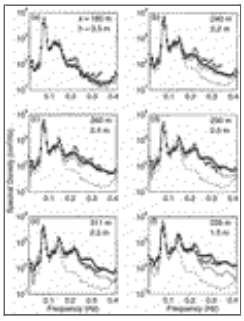

Click on thumbnail for full-sized image.

Fig. 7. Comparison of observed (solid curves) with predicted (asterisks: stochastic model, circles:deterministic model) spectra on 10 September at six instrument locations. The initial spectrum (H_s = 0.5 m) is indicated in each panel with a dashed curve.

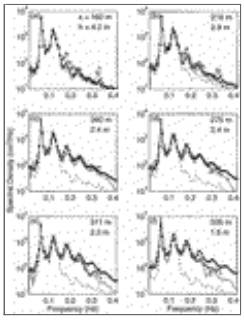

Click on thumbnail for full-sized image.

Fig. 8. Comparison of observed with predicted spectra on 15 September (H_s = 0.4 m) (same format as Fig. 7).

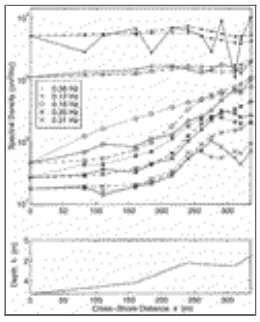

Click on thumbnail for full-sized image.

Fig. 9. Cross-shore evolution of the spectral levels (upper panel) at the peak frequency and the first four harmonic frequencies on 15 September. The solid curves are the observed levels, and the dotted and dashed curves are the deterministic and stochastic model predictions, respectively. The beach profile is shown in the lower panel.

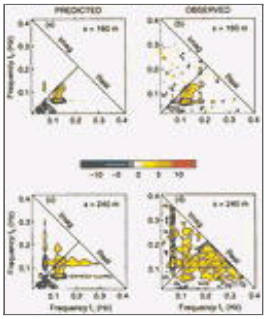

Click on thumbnail for full-sized image.

Fig. 10. Bispectra predicted with the stochastic model (left panels) and observed (right panels) offshore of the bar (x = 160 m, upper panels) and on the bar crest (x = 240 m, lower panels) on 15 September. The format of the panels is the same as in Fig. 2.

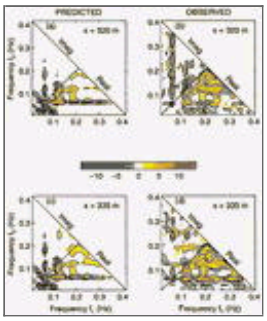

Click on thumbnail for full-sized image.

Fig. 11. Bispectra predicted with the stochastic model (left panels) and observed (right panels) on 15 September at x = 320 m (upper panels) and x = 335 m (lower panels). Both locations are on the beachface within about 50 m of the shoreline. The format of the panels is the same as in Fig. 2.

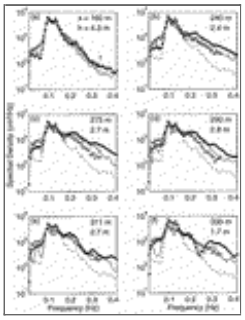

Click on thumbnail for full-sized image.

Fig. 12. Comparison of observed with predicted spectra on 24 September (H_s = 0.8 m) (same format as Fig. 7).

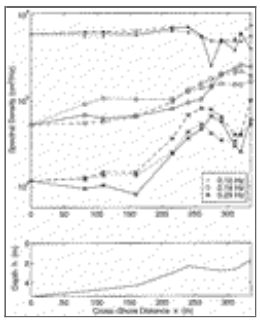

Click on thumbnail for full-sized image.

Fig. 13. Cross-shore evolution of the spectral levels (upper panel) at the peak frequency and the first two harmonic frequencies on 24 September (same format as Fig. 9). The beach profile is shown in the lower panel.

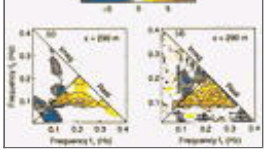

Click on thumbnail for full-sized image.

Fig. 14. Bispectra predicted with the stochastic model (left panels) and observed (right panels) on the bar crest (x = 240 m, upper panels) and inshore of the bar crest (x = 290 m, lower panels) on 24 September. The format of the panels is the same as in Fig. 2.

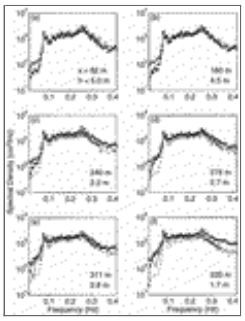

Click on thumbnail for full-sized image.

Fig. 15. Comparison of observed with predicted spectra on 21 September (H_s = 0.8 m) (same format as Fig. 7).

Corresponding author address: Dr. Thomas H. C. Herbers, Department of Oceanography, Code OC/He, Naval Postgraduate School, Monterey, CA 93943-5122.

E-mail: herbers@oc.nps.navy.mil

top